Toward high-energy-density, high-efficiency, and moderate-temperature chip-scale thermophotovoltaics

Walker R. Chan[a,b], Peter Bermel[a,b,c,d], Robert C. N. Pilawa-Podgurski[e], Christopher H. Marton[f], Klavs F. Jensen[f], Jay J. Senkevich[b], John D. Joannopoulos[a,b,c,d,1], Marin Soljačić[a,b,c,d], and Ivan Celanovic[b,1]

[a]Research Laboratory of Electronics, [b]Institute for Soldier Nanotechnologies, [c]Department of Physics, [d]Center for Materials Science and Engineering, and [f]Department of Chemical Engineering, Massachusetts Institute of Technology, Cambridge, MA 02139; and [e]Department of Electrical and Computer Engineering, University of Illinois at Urbana–Champaign, Urbana, IL 61801

Contributed by John D. Joannopoulos, January 24, 2013 (sent for review November 27, 2012)

The challenging problem of ultra-high-energy-density, high-efficiency, and small-scale portable power generation is addressed here using a distinctive thermophotovoltaic energy conversion mechanism and chip-based system design, which we name the microthermophotovoltaic (μTPV) generator. The approach is predicted to be capable of up to 32% efficient heat-to-electricity conversion within a millimeter-scale form factor. Although considerable technological barriers need to be overcome to reach full performance, we have performed a robust experimental demonstration that validates the theoretical framework and the key system components. Even with a much-simplified μTPV system design with theoretical efficiency prediction of 2.7%, we experimentally demonstrate 2.5% efficiency. The μTPV experimental system that was built and tested comprises a silicon propane microcombustor, an integrated high-temperature photonic crystal selective thermal emitter, four 0.55-eV GaInAsSb thermophotovoltaic diodes, and an ultra-high-efficiency maximum power-point tracking power electronics converter. The system was demonstrated to operate up to 800 °C (silicon microcombustor temperature) with an input thermal power of 13.7 W, generating 344 mW of electric power over a 1-cm^2 area.

catalytic combustion | micro generator | thermal radiation

With the recent proliferation of power-hungry mobile devices, significant research efforts have been focused on developing clean, quiet, and portable high-energy-density, compact power sources. Although batteries offer a well-known solution, limits on the chemistry developed to date constrain the energy density to ~0.2 kWh/kg, whereas many hydrocarbon fuels have energy densities closer to 12 kWh/kg. The fundamental question is, How efficiently and robustly can these widely available chemical fuels be converted into electricity in a millimeter-scale system? Indeed, it is difficult to tap the full potential of hydrocarbon fuels on a small scale. However, their high energy density allows even relatively inefficient generators to be competitive with batteries. To this end, researchers have explored different energy conversion routes, such as mechanical heat engines (1), fuel cells (2, 3), thermoelectrics (4, 5), and thermophotovoltaics (TPVs) (6, 7).

TPVs present an extremely appealing approach for small-scale power sources due to the combination of high power density limited ultimately by Planck blackbody emission, multifuel operation due to the ease of generating heat, and a fully static conversion process. Small-scale TPVs have yet to be demonstrated and are particularly challenging because of the need to develop strong synergistic interactions between chemical, thermal, optical, and electrical domains, which in turn give rise to requirements for extreme materials performance and subsystems synchronization.

In this work, we present a proof of concept microthermovoltaic (μTPV) system, shown in Fig. 1, that validates the theoretical foundation and paves the way toward a new breed of ultra-high-energy-density, high-efficiency, propane-fueled, chip-scale power sources. Specifically, our system comprises a catalytic microcombustor with a high-temperature photonic crystal for efficient conversion of heat into spectrally confined thermal radiation, optically coupled to low-bandgap photovoltaic (PV) diodes that are electrically interfaced with a unique ultra-low-power, on-chip power electronics converter, providing an optimal interface to external electrical loads.

Each of these four key components can be optimized for maximum performance with various degrees of complexity and difficulty. For simplicity, we shall begin our discussion with a simple and easily realizable μTPV materials system. A general theoretical formalism is then introduced that can accurately model these components, explore how they can work together, and provide optimized design within a constrained geometric and materials space. This also helps provide experimental validation of this approach. Indeed, as we shall see, the predicted efficiency of this simple μTPV system is 2.7%, whereas our results give 2.5%. Finally, the theoretical framework will be used to present a detailed optimized design using advanced material systems, system geometry, and PV cells. This optimized theoretical design boasts efficiencies that exceed 30% heat-to-electricity conversion.

Simple Silicon μTPV

The starting point for any portable TPV system is a compact mechanism for generating heat. Our basic μTPV, shown in Fig. 1, catalytically combusts hydrocarbon fuel (i.e., propane) inside a catalyst-coated Si microchannel structure. The microreactor is designed to minimize nonradiative thermal losses by suspending it with glass capillary tubes that double as fluidic connections and vacuum packaging. In this design we use pure oxygen, instead of air, for the chemical reaction, to simplify the test and characterization. Thermal energy generated from chemical reaction inside the reactor heats up the Si and is consequently converted into spectrally confined radiative heat by a one-dimensional (1D) Si/SiO_2 photonic crystal that serves as a narrow-band thermal emitter.

To convert thermal radiation into electricity, we use low-bandgap PV cells made from $Ga_{1-x}In_xAs_{1-y}Sb_y$ ($x = 0.15, y = 0.12$), grown by metalorganic vapor phase epitaxy (MOVPE), with a bandgap of 0.547 eV. They consist of a 1-μm n-GaInAsSb base, a 4-μm p-GaInAsSb emitter, an AlGaAsSb window layer, and a GaSb contact layer on an n-GaSb substrate. Further details of the design and performance parameters are given in refs. 8–10.

In the final conversion step, the raw output of the TPV cell is dynamically converted into useful current and voltage levels via a low-power power electronics converter known as the maximum power-point tracker (MPPT). This step is important because the generator operating conditions (i.e., incident irradiation and the cell junction temperature) can vary over time and must therefore be continuously tracked to ensure that maximum power is extracted from the cells at all times. The extraordinarily small

Author contributions: W.R.C., P.B., R.C.N.P.-P., C.H.M., K.F.J., J.J.S., J.D.J., M.S., and I.C. designed research, performed research, analyzed data, and wrote the paper.

The authors declare no conflict of interest.

Freely available online through the PNAS open access option.

[1]To whom correspondence may be addressed. E-mail: joannop@mit.edu or ivanc@mit.edu.

Report Documentation Page

Form Approved
OMB No. 0704-0188

1. REPORT DATE	2. REPORT TYPE	3. DATES COVERED
02 APR 2013		**00-00-2013 to 00-00-2013**

4. TITLE AND SUBTITLE	5a. CONTRACT NUMBER
Toward high-energy-density, high-efficiency, and moderate-temperature chip-scale thermophotovoltaics	5b. GRANT NUMBER
	5c. PROGRAM ELEMENT NUMBER
6. AUTHOR(S)	5d. PROJECT NUMBER
	5e. TASK NUMBER
	5f. WORK UNIT NUMBER
7. PERFORMING ORGANIZATION NAME(S) AND ADDRESS(ES) **Massachusetts Institute of Technology,Research Laboratory of Electronics,77 Massachusetts Avenue,Cambridge,MA,02139**	8. PERFORMING ORGANIZATION REPORT NUMBER
9. SPONSORING/MONITORING AGENCY NAME(S) AND ADDRESS(ES)	10. SPONSOR/MONITOR'S ACRONYM(S)
	11. SPONSOR/MONITOR'S REPORT NUMBER(S)

12. DISTRIBUTION/AVAILABILITY STATEMENT
Approved for public release; distribution unlimited

13. SUPPLEMENTARY NOTES

14. ABSTRACT

15. SUBJECT TERMS

16. SECURITY CLASSIFICATION OF:			17. LIMITATION OF ABSTRACT	18. NUMBER OF PAGES	19a. NAME OF RESPONSIBLE PERSON
a. REPORT **unclassified**	b. ABSTRACT **unclassified**	c. THIS PAGE **unclassified**	**Same as Report (SAR)**	**6**	

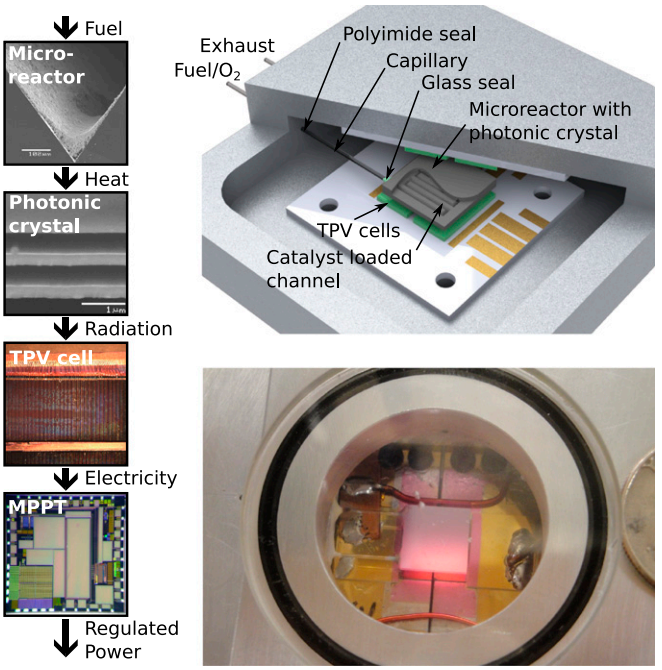

Fig. 1. (*Left*) General operation of a fuel-based μTPV system. It uses a microreactor to catalytically combust propane; the heat is quickly conducted to the photonic crystal emitter at the surface, which selectively emits thermal photons, across a gap, toward a target TPV cell. The raw electrical output is then optimized and regulated by our maximum power-point tracker. (*Upper Right*) Labeled CAD model of our experimental μTPV system. (*Lower Right*) Photograph of our experimental μTPV in operation.

size of the overall system in this work makes it particularly difficult to ensure perfect TPV cell-current matching, owing to cavity reflections and uneven irradiation across the different cells. Unfortunately, any irradiation mismatch between cells will limit the current through a series-connected string of cells to that of the weakest cell, causing a lower output power than what is theoretically possible. Ref. 11 describes a method that employs distributed intelligent power electronics to mitigate the effects of cell mismatch. By using multiple low-power, low-voltage MPPTs, we individually control each section of the cell array to operate at its most efficient point. The distributed MPPT architecture optimizes the electrical output of the TPV cells in real time to continuously track the maximum power point, irrespective of uneven irradiation and any changes in the heat-source operation.

Theoretical Framework

Converging the four coupled energy conversion technologies (microreactor, selective thermal emitter, low-bandgap PV diode, and low-power power electronics converter) and achieving high overall system performance requires accurate system-level modeling (including ab initio calculations for each component), followed by multidimensional constrained global optimization of the design parameters. We modeled the microreactor with custom heat transfer code incorporating conduction, convection, and radiative heat transfer between surfaces and into the ambient. We account for radiation from the two sides facing the cells and the edges, conduction through the Pyrex tubes, and heat carried out by the hot exhaust gases. We use the transfer matrix method (12, 13) to calculate the angular-dependent emissivity for a given structure, as discussed in ref. 14. Then we use ray optics to accurately incorporate multiple scattering effects, as discussed in ref. 15. Our heat transfer and diode modeling codes discussed elsewhere were used to calculate electrical power. The operating temperature is calculated using a self-consistent nonlinear Newton–Raphson method solver.

One of the most significant loss mechanisms for TPV systems is thermal radiation of photons below the electronic bandgap of the TPV diode. Recent literature points to the potential for spectral shaping and photon recycling to dramatically reduce the losses associated with below-bandgap photons (14, 16–25), enabled by photonic crystals (26, 27). To explore some design limits on the performance of our μTPV systems, we model two simple emitters, assuming maximally efficient recuperators and a view factor of 100%. They consist of a baseline design with a homogeneous greybody Si emitter and an optimized 1D metallodielectric photonic crystal design. The photonic crystal emitter shapes the radiated spectrum, maximizing the efficiency by suppressing unconvertible radiation. In addition, the photonic crystal (PhC) emitter enables the use of a lower-temperature (700–1,100 °C) emitter, resulting in reduced thermal stresses, a larger spectrum of available materials, and better material stability, thus extending the possible design space. The photonic crystal design parameters were chosen via constrained global optimization of the figure of merit, as described in ref. 14. The results that show output power as a function of input chemical power are given in Fig. 2*A*, and the efficiency as a function of microreactor surface temperature is given in Fig. 2*B*. It can be observed that for a constant input power, the projected efficiency of the 1D metallic photonic crystal exceeds that of the uniform greybody Si emitter by approximately a factor of 3, as shown in Fig. 2. This alone demonstrates the importance of photonic crystals as an enabling technology for μTPV and TPV systems in general.

As we shall see below, high-temperature material stability and reactivity of the Si reactor prompt the use of a Si-based photonic crystal thermal emitter.

Experimental Results for Two Silicon Reactor Designs

The theoretical formalism developed can accurately predict the losses for a simple μTPV system comprising a greybody Si emitter operating at ~700 °C with a view factor of 70% and a GaInAsSb cell mentioned above, as in ref. 10. Approximately 12% losses come from heat exhaust in the absence of a recuperator (when oxygen is used as oxidizer instead of air; with air as oxidizer these losses would be higher); 24% losses from radiation losses off to the side; 60% from low-energy photons that cannot be converted into electricity; and 3% from the operation of the thermophotovoltaic cell, including shadowing, open-circuit voltage degradation, hot-carrier thermalization, and radiative recombination at the maximum power point. Thus, this straightforward design will only operate at an efficiency of ~1%, corresponding to the experimental results further discussed below, and also shown in Fig. 3. It should be emphasized that this result is obtained without any need for curve fitting (i.e., purely from first principles). From this analysis, it is clear that the most important area for improvement is in reducing the energy emitted as low-energy photons via photonic crystals. Other important changes include adding a recuperator to recover thermal power from the exhaust and increasing the view factor to eliminate losses off to the sides.

The theoretical formalism can also be used to further optimize the parameters of the simple Si μTPV system with the constraint that only Si and SiO_2 are used as materials for 1D selective emitter design on the surface of the reactor. Indeed, a 1D photonic crystal consisting of five alternating layers of Si and SiO_2 is chosen for its ease of fabrication and high-temperature compatibility with the Si microreactors. In Fig. 4 we show the thermal emission results of 1D photonic crystal consisting of five alternating layers of Si and SiO_2, with a total thickness of ~2 μm. The materials were chosen for ease of fabrication and compatibility with the Si microreactor. We measured the thermal emission of the photonic crystal by electrically heating it and measuring the emitted spectrum by FTIR spectroscopy. The three spectra shown in Fig. 4 exhibit good agreement between theory and experiment

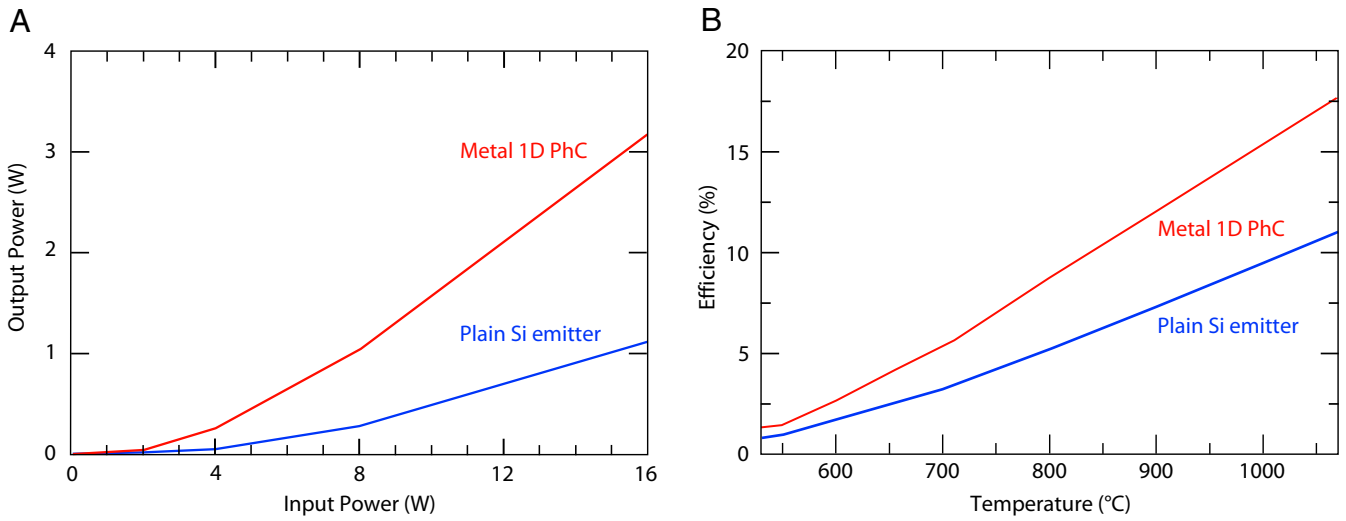

Fig. 2. (*A*) Electrical power output as a function of chemical input power of μTPV system designs with two types of emitters: Si greybody in blue and optimized 1D metallodielectric PhC in red. (*B*) Efficiency as a function of microreactor temperature for μTPV system designs with two types of emitters: Si greybody in blue, and optimized 1D metallodielectric PhC in red. Note that for a constant input power, the operating temperature of the plain emitter is lower than that of the 1D PhC. For example, the input power of the plain emitter at 700 °C corresponds to that of the 1D PhC at 830 °C.

(simulation results took into account temperature-dependent dielectric functions of Si and SiO_2). We used high-performance TPV cells made from $Ga_{1-x}In_xAs_{1-y}Sb_y$ ($x = 0.15, y = 0.12$), grown by MOVPE, with a bandgap of 0.547 eV. They consist of a 1-μm n-GaInAsSb base, a 4-μm p-GaInAsSb emitter, a AlGaAsSb window layer, and a GaSb contact layer on an n-GaSb substrate. The measured external quantum efficiency (ratio of electron-hole generation to incident photons) of the cells with a four-layer antireflective coating is plotted in Fig. 4.

In Fig. 3 we show our results for the complete system. Our numerical model predictions are shown as solid lines, and the corresponding experimental data points are shown as symbols with the same color as the predictive curve. The excellent point-by-point match between the two curves obtained without curve fitting validates our model and provides confidence in our theoretical

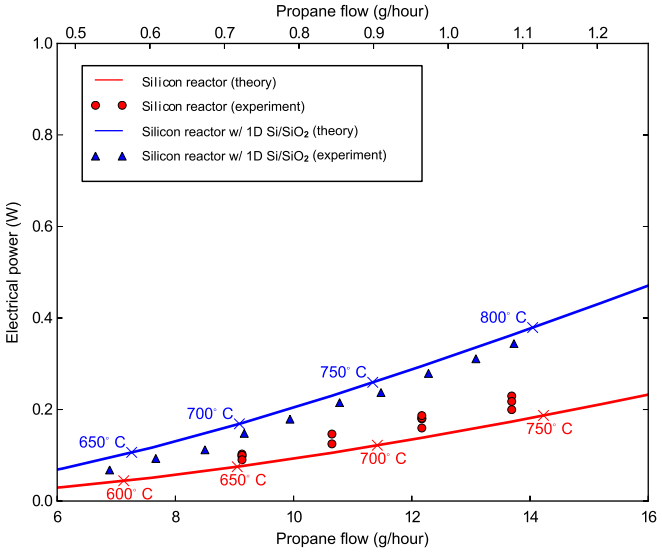

Fig. 3. Theoretical and experimental performance of our TPV system with two emitters: bare Si and 1D Si/SiO_2 photonic crystal. Calculated microreactor temperatures are labeled.

formalism. For the experimental results we tested the complete system by first igniting the microreactor by hydrogen-assisted combustion of propane in oxygen until a temperature of 400 °C was reached. Above that temperature, the propane kinetics over the catalyst were sufficient for autothermal operation, and the hydrogen flow was shut off. The propane and oxygen flows were gradually increased in small increments, with 1.5 times the stoichiometric amount of oxygen required for complete combustion. We plot the steady-state electrical power at the maximum power point versus propane flow in Fig. 3. The propane flow was converted to watts using the lower heating value. We tested the system both with a simple Si reactor and a Si reactor with a photonic crystal. The simple Si-based system (without selective emitter) generated a maximum 218 mW of electricity with 13.7 W of propane flow, at an efficiency of 1.6% at 740 °C. Note that at a lower temperature (or flow) the efficiency is reduced; for example, at ~700 °C the efficiency goes down to 1.2%. The μTPV system with a 1D Si/SiO_2 photonic crystal generated 344 mW of electricity under the same conditions at an efficiency of 2.5%, whereas the predicted efficiency was 2.7%. Furthermore, according to our model, the thermal losses of our system under typical operating conditions are distributed as follows: 10% exhaust, 40% radiation loss off the edges of the microreactor or the sides of the vacuum gap, and 50% dissipation in the TPV cells due to below-bandgap radiation, thermalization, and electrical losses. The fabrication and testing procedures used to obtain these results are outlined in *Materials and Methods*.

In Fig. 5 we show the results for an idealized μTPV system with perfectly reflective microburner sides, a 2D tungsten PhC slab consisting of a square lattice of air holes, and multilayer dielectric filter (14) in front of the PV cell, and a perfect recuperator. In Fig. 5, we plot the efficiency as a function of operating temperature. The results are very striking: 20% efficiency is possible around 700 °C and over 30% efficiency above 1,000 °C.

To realize a microreactor with metal-coated edges, a high-temperature, highly reflective metallic coating, compatible with a Si platform, would need to be developed. This coating would also need to possess a robust high-temperature diffusion barrier. An alternative path would be to design and fabricate the microreactor completely out of metal, thus inherently leading to low-emissivity side walls.

Use of metallic photonic crystals as selective thermal emitters could possibly be accomplished via either thin-film deposition

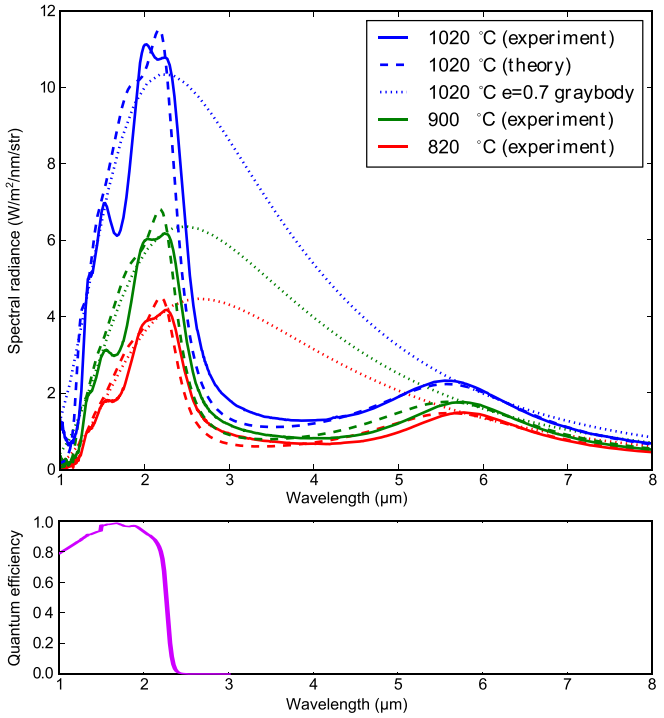

Fig. 4. (*Upper*) Measured and simulated thermal emission, normal to the surface, of the photonic crystal at 820, 900, and 1,020 °C plotted with solid and dashed lines, respectively. Simulation results of three graybody emitters with 0.7 emittance (approximation of Si emittance), at 820, 900, and 1,020 °C are shown with dotted lines. (*Lower*) Measured external quantum efficiency (EQE) for the GaInAsSb PV cell with antireflective coating.

and etching in a Si platform or by building the reactor out of high-temperature metal. Use of higher-dimensional photonic crystals (2D and 3D) could be accomplished via layer-by-layer microfabrication techniques onto a Si or metallic reactor (26). To incorporate selective filters into a μTPV generator, precise and robust thin-film deposition and packaging processes will be needed that will allow for direct deposition of filters onto the front surface of the PV cell. A smaller distance gap between the microreactor and the PV cell (close to unity view factor) could be achieved with a new mechanical design and assembly approach.

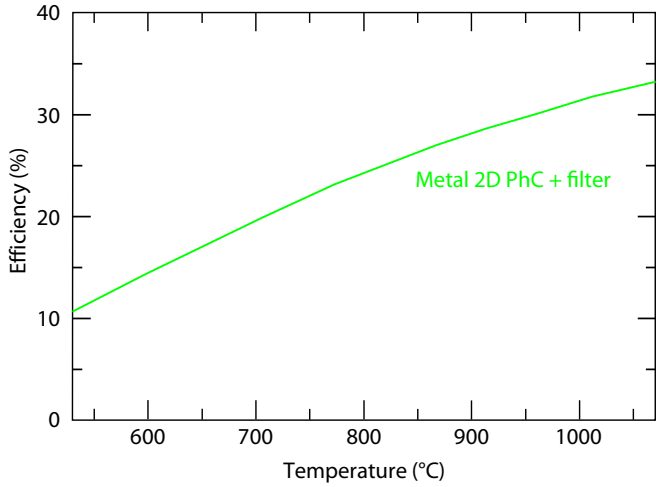

Fig. 5. Theoretical limits on performance of μTPV system designs with optimized 2D tungsten PhC.

Finally, high-efficiency, small-scale recuperators will need to be integrated into the reactor platform as an additional subsystem.

Conclusion and Summary

In conclusion, with our prototype μTPV system, and accurate system-level modeling verified by experiment, we have demonstrated the intriguing potential of μTPV technology. Based on the experimental fuel flow rate and calculated limit of 32% efficiency for our millimeter-scale form factor, and adjusting for likely real-world losses, it should be possible to create compact generators with electrical outputs from milliwatts to few tens of watts (electrical power) with power densities exceeding 0.5 W/cm^2 and energy densities over 3 kWh/kg. Enabling technologies required to achieve this performance include advanced photonic crystal fabrication, higher-performance low-bandgap PV cells, vacuum packaging, and high-efficiency microreactor and recuperator designs. Indeed, we believe μTPV generators represent a very attractive alternative to batteries, portable fuel cells, and thermoelectric technologies for portable power generation.

Materials and Methods

Microreactor. The heat source in our TPV system was a microreactor developed by Brandon Blackwell (28) and based on previous work by the same group (29, 30). The microreactor was a 10- × 10- × 1.3-mm Si slab with a 0.40-mm square serpentine channel defined by potassium hydroxide etching and Si fusion bonding using standard microfabrication techniques. The channel was coated with a platinum catalyst because at this length scale radical and thermal quenching at the walls prevents stable homogeneous combustion (31). Catalytic combustion offers another benefit: The combustion happens at the channel walls, where heat is directly conducted through the Si to the selective emitter.

The catalyst was applied as a washcoat after the devices were diced but before the capillary tubes were attached. We used a 20 wt% suspension of 5 wt% platinum on porous alumina (311324; Sigma-Aldrich) in a 2 wt% solution of a nitrocellulose in amyl acetate. The suspension was sucked through the channel. After the solvent dried, a thin coating of catalyst was glued to the walls by the nitrocellulose, which was subsequently burned out. Nitrocellulose can decompose to gaseous byproducts without air, which is unavailable deep in the serpentine structure. The catalyst solution and loading method were tweaked to constantly deposit about 1 mg of catalyst. An SEM micrograph of the catalyst is shown in Fig. 1 *Inset*.

The microreactor was supported by two Pyrex capillary tubes that also served as fluidic connections to the channel to minimize conductive heat loss. The two 0.55-mm o.d. × 0.40-mm i.d. × 12-mm-long capillaries were hermetically sealed to the microreactor with a glass solder (SEM-COM SCC-7). The powdered solder glass was mixed with a solution of 1 wt% nitrocellulose in isophorone and carefully applied to the joint with a fine wire while the microreactor and tubes were held in a jig. The ratio of powder to solvent was determined empirically. The firing cycle was based on the manufacturer's recommendations, the literature (32, 33), a differential scanning calorimetry analysis of the glass solder, and trial and error. The finished microreactor and tubes were sealed to the vacuum package shown in Fig. 1 with a polyimide adhesive (Imitec).

The microreactor was initially in a setup similar to that shown in Fig. 1 without cells and with an IR window replacing the top cells. We measured the temperature of a microreactor without a photonic crystal with an IR thermometer (G5L; Optris) sensitive to 5-μm thermal radiation that was calibrated with temperature-indicating lacquer (OmegaLaq). The average surface temperature reached about 800 °C when burning 10 standard cubic centimeters per minute (sccm) of propane and 75 sccm of oxygen. The microreactor with the photonic crystal can reach the same temperature with less fuel consumption owing to lower heat loss, although IR thermometry was difficult because of the wavelength-dependent emissivity.

The cutoff in the experimental performance for the measured μTPV generators in Fig. 3 at 1.1 g/h (8 sccm) propane flow was most likely caused by softening of the joint between the microreactor and the capillary as it approaches the transition temperature of the glass solder.

In future work, a joint capable of operating at higher temperatures would be highly desirable. Additionally, a combustor that burns in air rather than pure oxygen is necessary, because carrying both the fuel and oxidizer goes against the goal of high energy density. It should be possible to design a new microreactor that can reach the necessary temperatures with propane–air combustion. Although burning with air has the disadvantage of increasing the exhaust enthalpy loss five times at a given microreactor

temperature, using a recuperator to transfer heat from the exhaust to the incoming air would bring the losses down to a reasonable level.

Photonic Crystal. The polycrystalline Si and SiO_2 structure arrived at by the optimization process was deposited by low-pressure and plasma-enhanced chemical vapor deposition, respectively, directly on the microreactors. The wafer was annealed after each deposition. The deposition was done after wafer bonding but before die sawing. As a result, the edges of the microreactors are uncoated. A SEM micrograph of the structure is in the upper-left inset of Fig. 1.

We measured the thermal emission of the photonic crystal by electrically heating it and measuring the emitted spectrum by FTIR spectroscopy. The FTIR and the optics used to convey the light were calibrated with a standard blackbody source. The measurement was performed at three different power levels. The temperature of the sample was estimated from a model because it proved impractical to measure the temperature directly. The three spectra are shown in Fig. 4. The photonic crystal is able to improve efficiency by suppressing radiation between 2.5 and 5.5 μm. Suppressing this radiation approximately doubles the efficiency of the system as a whole.

TPV Cells. We modeled our cells with an equivalent circuit model with temperature- and illumination-dependent circuit elements. We fit the equivalent circuit to the cell's current voltage data. Then we verified the model by illuminating the cell with a calibrated blackbody source and comparing the measured and calculated performance. The modeling is described in ref. 10.

The cells were mounted to a copper core printed circuit board (Bergquist) used in the power electronics industry by fluxless indium reflow soldering. The solder joint was inspected with scanning acoustic microscopy and found to be free of large voids. The solder joint serves as both a thermal connection to the substrate and as the negative electrical contact. The positive electrical contact was made to the bus bar by wire bonding. An SiO_2/Ta_2O_5/Si antireflective coating was deposited on the packaged devices. The finished cells were mounted on temperature-controlled water-cooled blocks above and below the microreactor in the experimental apparatus in Fig. 1.

Maximum Power-Point Tracker. The prototype MPPT pictured in Fig. 1 was used to successfully demonstrate the system operation in ref. 11. More recent work (34) has focused on reducing the overall size of the power electronics to fit in a small form factor, as well as to increase the electrical conversion efficiency. Shown in the bottom left corner of Fig. 1 is a die photo of the fully integrated MPPT developed in a 0.35-μm CMOS process to interface the TPV system with the load. Table 1 lists the electrical specifications of the MPPT. In the table, the tracking efficiency is a measure of how close the power converter can operate to the ideal maximum power point.

Table 1. MPPT specifications

Parameter	Value
Input voltage range	0.8–1.3 V (1 V nominal)
Output voltage range	3.6–4.2 V (4 V nominal)
Nominal output power	300 mW
Switching frequency	500 kHz
Converter peak efficiency	95.4%
Tracking efficiency	>98%

It should be noted that the low-voltage distributed MPPT architecture developed for this work is not limited to only this application. Other applications that might benefit from system-level efficiency improvements through the use of this architecture include concentrated solar photovoltaics, thermoelectrics, and fuel cells.

System Testing. The microreactor was ignited by hydrogen-assisted combustion of propane until a temperature of 400 °C was reached. Above that temperature, the propane kinetics over the catalyst were sufficient for autothermal operation, and the hydrogen flow was shut off. The propane and oxygen flows were gradually increased in small increments with our mass flow controllers, with 1.5 times the stoichiometric amount of oxygen required for complete combustion. The system was allowed to reach steady state after each flow increase. At each point, we recorded the input flow and output powers, as shown in Fig. 3. Output power was found by performing a current-voltage sweep on a Keithley source meter and calculating the maximum power. Efficiency is defined as the ratio of the input and output powers, where input power is given by the propane flow rate times the lower heating value.

ACKNOWLEDGMENTS. We thank Dr. W. A. Peters for a critical reading of the manuscript. This research was supported in part by the US Army Research Office through the Institute for Soldier Nanotechnologies under Contract W911NF-07-D-0004. W.R.C., J.J.S., and M.S. were partially supported by the Massachusetts Institute of Technology Solid State Solar Thermal Energy Conversion Energy Research Frontier Center of the Department of Energy under Grant DE-SC0001299.

1. Aichlmayr H, Kittelson D, Zachariah M (2002) Miniature free-piston homogeneous charge compression ignition engine-compressor conceptpart i: Performance estimation and design considerations unique to small dimensions. *Chem Eng Sci* 57:4161–4171.
2. Kundu A, et al. (2007) Micro-fuel cells current development and applications. *J Power Sources* 170:67–78.
3. Cowey K, Green K, Mepsted G, Reeve R (2004) Portable and military fuel cells. *Curr Opin Solid State Mater Sci* 8:367–371.
4. Yoshida K, Tanaka S, Tomonari S, Satoh D, Esashi M (2006) High-energy density miniature thermoelectric generator using catalytic combustion. *J Microelectromech Syst* 15: 195–203.
5. Marton CH, Haldeman GS, Jensen KF (2011) Portable thermoelectric power generator based on a microfabricated silicon combustor with low resistance to flow. *Ind Eng Chem Res* 50:8468–8475.
6. Fraas LM, Avery JE, Huang HX (2003) Thermophotovoltaic furnace generator for the home using low bandgap gasb cells. *Semicond Sci Technol* 18:S247.
7. Doyle E, Shukla K, Metcalfe C (2001) Development and demonstration of a 25 watt thermophotovoltaic power source for a hybrid power system. National Aeronautics and Space Administration, Technical Report TR04-2001. Available at http://ntrs.nasa.gov/search.jsp?R=20010093213.
8. Wang CA, et al. (1999) High-quantum-efficiency 0.5eV GaInAsSb/GaSb thermophotovoltaic devices. *Appl Phys Lett* 75:1305–1307.
9. Dashiell MW, et al. (2006) Quaternary InGaAsSb thermophotovoltaic diodes. Electron Devices. *IEEE Transactions on* 53:2879–2891.
10. Chan W, et al. (2010) Modeling low-bandgap thermophotovoltaic diodes for high-efficiency portable power generators. *Sol Energy Mater Sol Cells* 94:509–514.
11. Pilawa-Podgurski RCN, Pallo NA, Chan WR, Perreault DJ, Celanovic IL (2010) Low-power maximum power point tracker with digital control for thermophotovoltaic generators. *Twenty-Fifth Annual IEEE Applied Power Electronics Conference and Exposition (APEC)* (IEEE, Piscataway, NJ), pp 961–967.
12. Li L (1996) Formulation and comparison of two recursive matrix algorithms for modeling layered diffraction gratings. *J Opt Soc Am A Opt Image Sci Vis* 13:1024–1035.
13. Whittaker D, Culshaw I (1999) Scattering-matrix treatment of patterned multilayer photonic structures. *Phys Rev B* 60:2610–2618.
14. Bermel P, et al. (2010) Design and global optimization of high-efficiency thermophotovoltaic systems. *Opt Express* 18(Suppl 3):A314–A334.
15. Eckert E, Sparrow E (1961) Radiative heat exchange between surfaces with specular reflection. *Int J Heat Mass Transfer* 3:42–54.
16. O'Sullivan F, et al. (2005) Optical characteristics of 1d si/sio$_2$ photonic crystals for thermophotovoltaic applications. *J Appl Phys* 97:033529.
17. Heinzel A, et al. (2000) Radiation filters and emitters for the nir based on periodically structured metal surfaces. *J Mod Opt* 47(13):2399–2419.
18. Gee JM, Moreno JB, Lin SY, Fleming JG (2002) Selective emitters using photonic crystals for thermophotovoltaic energy conversion. *Conference Record of the Twenty-Ninth IEEE Photovoltaic Specialists Conference 2002* (IEEE, Piscataway, NJ), pp 896–899.
19. Sai H, Kanamori Y, Yugami H (2003) High-temperature resistive surface grating for spectral control of thermal radiation. *Appl Phys Lett* 82:1685–1687.
20. Ortabasi U, Bovard B (2003) Rugate technology for thermophotovoltaic applications: a new approach to near perfect filter performance. *AIP Conf Proc* 653: 249–258.
21. Celanovic I, Perreault D, Kassakian J (2005) Resonant-cavity enhanced thermal emission. *Phys Rev B* 72:075127.
22. Chan DL, Celanovic I, Joannopoulos JD, Soljacic M (2006) Emulating one-dimensional resonant *q*-matching behavior in a two-dimensional system via fano resonances. *Phys Rev A* 74:064901.
23. Celanovic I, Jovanovic N, Kassakian J (2008) Two-dimensional tungsten photonic crystals as selective thermal emitters. *Appl Phys Lett* 92:193101.
24. Rahmlow TD, et al. (2007) Development of front surface, spectral control filters with greater temperature stability for thermophotovoltaic energy conversion. *AIP Conf Proc* 890:59–67.
25. John S, Wang R (2008) Metallic photonic band-gap filament architectures for optimized incandescent lighting. *Phys Rev A* 78:043809.
26. Fleming JG, Lin SY, El-Kady I, Biswas R, Ho KM (2002) All-metallic three-dimensional photonic crystals with a large infrared bandgap. *Nature* 417(6884):52–55.
27. Joannopoulos JD, Johnson SG, Winn JN, Meade RD (2008) *Photonic Crystals: Molding the Flow of Light* (Princeton Univ Press, Princeton), 2nd Ed.
28. Blackwell BS (2008) Design, fabrication, and characterization of a micro fuel processor. PhD thesis (Massachusetts Institute of Technology, Cambridge, MA).
29. Nielsen O (2006) A thermally efficient micro-reactor for thermophotovoltaic power generation. PhD thesis (Massachusetts Institute of Technology, Cambridge, MA).

30. Arana L (2003) High-temperature microfluidic systems for thermally-efficient fuel processing. PhD thesis (Massachusetts Institute of Technology, Cambridge, MA).
31. Fernandez-Pello AC (2002) Micropower generation using combustion: Issues and approaches. *Proc Combust Inst* 29:883–899.
32. Forbes DWA (1967) Solder glass seals in semi-conductor packaging. *Glass Technol* 8 (2):32–42.
33. Frieser RG (1975) A review of solder glass. *Electrocomponent Sci Technol* 2: 163–199.
34. Pilawa-Podgurski RCN, Li W, Celanovic I, Perreault DJ (2011) Integrated cmos dc-dc converter with digital maximum power point tracking for a portable thermophotovoltaic power generator. *IEEE Energy Conversion Congress and Exposition (ECCE)* (IEEE, Piscataway, NJ), pp 197–204.